Hindawi
International Journal of Photoenergy
Volume 2018, Article ID 8654963, 7 pages
https://doi.org/10.1155/2018/8654963

Research Article

Fabrication and Characterization of $CH_3NH_3PbI_3$ Perovskite Solar Cells Added with Polysilanes

Takeo Oku,[1] **Junya Nomura**,[1] **Atsushi Suzuki**,[1] **Hiroki Tanaka**,[1] **Sakiko Fukunishi**,[2] **Satoshi Minami**,[2] **and Shinichiro Tsukada**[2]

[1]*Department of Materials Science, The University of Shiga Prefecture, Hikone, Shiga 522-8533, Japan*
[2]*Frontier Materials Laboratories, Osaka Gas Chemicals Co., Ltd., Osaka 554-0051, Japan*

Correspondence should be addressed to Takeo Oku; oku@mat.usp.ac.jp

Received 6 July 2018; Revised 24 August 2018; Accepted 1 September 2018; Published 2 October 2018

Academic Editor: Věra Cimrová

Effects of polysilane additions on $CH_3NH_3PbI_3$ perovskite solar cells were investigated. Photovoltaic cells were fabricated by a spin-coating method using perovskite precursor solutions with polymethyl phenylsilane, polyphenylsilane, or decaphenyl cyclopentasilane (DPPS), and the microstructures were examined by X-ray diffraction and optical microscopy. Open-circuit voltages were increased by introducing these polysilanes, and short-circuit current density was increased by the DPPS addition, which resulted in the improvement of the photoconversion efficiencies to 10.46%. The incident photon-to-current conversion efficiencies were also increased in the range of 400~750 nm. Microstructure analysis indicated the formation of a dense interfacial structure by grain growth and increase of surface coverage of the perovskite layer with DPPS, and the formation of PbI_2 was suppressed, leading to the improvement of photovoltaic properties.

1. Introduction

Inorganic-organic solar cells have been developed and studied as next-generation systems. Since organic thin-film solar cells have the advantages of low cost, flexibility, and being lightweight, the photovoltaic and optical properties of the organic solar cells have been studied [1–7]. Polysilane is a p-type semiconductor and has been used as an electrical conductive material and photovoltaic systems [7–14]. Polysilanes are known as σ-conjugate polymers, and their hole mobility is 10^{-4} cm^2 V^{-1} s^{-1} [7]. Although the polysilanes could be applied to p-type semiconductors on organic thin-film solar cells, few studies on polysilane-based solar cells have been reported [8, 14, 15].

Recently, inorganic-organic $CH_3NH_3PbI_3$-based perovskite solar cells have been widely studied because of its easy fabrication process and the high conversion efficiencies compared to the common organic solar cells [16–19]. After a conversion efficiency reached 15% in 2013 [20], higher efficiencies have been achieved for various processes and device structures, and the conversion efficiency increased above 20% [21–25]. The photovoltaic properties of the perovskite solar cells are fairly dependent on compositions and the crystal structures of the perovskite compounds. Halogen atom doping, such as bromine (Br) or chlorine (Cl), at the iodine (I) sites of the perovskite crystals have been investigated. The doped Cl ions could lengthen the diffusion length of excitons, which resulted in the improvement in the conversion efficiency [26–30]. In addition, studies on metal atom doping, such as tin (Sn) [31, 32], germanium [33, 34], antimony (Sb) [35–40], copper (Cu) [41–44], arsenic (As) [45], or thallium (Tl) [34], at the lead (Pb) sites have been performed. The optical absorption ranges of the perovskite solar cells were expanded by Sn or Tl doping [31, 32, 34], and the photoconversion efficiencies were improved by Sb-, Cu-, or As doping. Further doping of cesium [23], rubidium [24], or formamidinium ($NH{=}CHNH_3$) [21, 22] also improved the conversion efficiencies of the perovskite solar cells. Detailed studies on the elemental doping at the I, Pb, and/or CH_3NH_3 sites are fascinating for effects on

the photovoltaic properties and microstructures, and tolerance factors are also valuable to estimate stabilities of the perovskite crystals [46].

Carrier transport layers are also important for the improvement of the perovskite solar cells. Commercial 2,2′,7,7′-tetrakis[N,N-di-pmethoxyphenylamino]-9,9′-spirobifluorene (spiro-OMeTAD) has been normally used as the hole transport layers. However, spiro-OMeTAD is an expensive organic compound and not so much stable at elevated temperatures, which is one of the crucial issues for the development of the perovskite-type solar cells. In our previous works, several polysilanes have been applied for perovskite solar cells [47]. The conversion efficiencies of $CH_3NH_3PbI_3$-based solar cells using polysilane-doped hole transport layers were improved compared with those of a conventional $CH_3NH_3PbI_3$-based solar cells using spiro-OMeTAD.

The purpose of the present work is to investigate photovoltaic properties of $CH_3NH_3PbI_3$-based solar cells introduced with various polysilanes in the perovskite precursor solutions. Effects of polysilane addition on the photovoltaic properties were investigated by current density-voltage curves and incident photon-to-current conversion efficiencies. Microstructures of the thin films were investigated by X-ray diffraction (XRD) and optical microscopy.

2. Materials and Methods

Figure 1 shows a schematic illustration of fabricated device structure of the present photovoltaic devices. The detailed fabrication process is described in our previous reports [47–49], except for the process of polysilane doping into $CH_3NH_3PbI_3$ solutions. Fluorine-doped tin oxide- (FTO-) coated glass substrates were cleaned in an ultrasonic bath containing acetone and methanol. After rinsing with ultrapure water and drying under nitrogen gas, the substrates were treated with an ultraviolet-ozone cleaner (Asumi Giken Ltd., ASM 401N) for 15 min. For a compact TiO_2 layer, 0.15 and 0.30 M TiO_x precursor solutions were prepared from titanium diisopropoxide bis(acetylacetonate) (Sigma-Aldrich, 0.055 and 0.110 mL) as a solute and 1-butanol (Nacalai Tesque, 1 mL) as a solvent. The precursor solutions were stirred for 12 h at room temperature. The 0.15 M TiO_x precursor layer was spin-coated onto the cleaned FTO surface by a spin coater (Mikasa, MS-A100) at 3000 rpm for 30 s and was heated onto a hot plate (As One, ND-1) at 125°C for 5 min. Then, the 0.30 M TiO_x precursor layer was spin-coated on the 0.15 M TiO_x layer at 3000 rpm for 30 s. This process was repeated twice. After the spin-coating, the 0.30 M TiO_x layer was heated onto the hot plate at 125°C for 5 min. The TiO_x on the FTO was annealed in an electric furnace (As One, SMF-1) at 500°C for 30 min to form a compact TiO_2 layer. After cooling to room temperature, a mesoporous TiO_2 layer was spin-coated on the compact TiO_2 layer at 5000 rpm for 30 s, where the TiO_2 paste was prepared by diluting TiO_2 powder (Aerosil, P-25, 100 mg) in ultrapure water and adding poly(ethylene glycol) (molecular weight: 20000, Nacalai Tesque, 10 mg), acetylacetone (Sigma-Aldrich, 10 mL), and surfactant (Sigma-Aldrich, Triton X-100, 5 mL) for 30 min. After heating at 125°C for 5 min, the samples were annealed in the electric furnace at 500°C for 30 min. For the preparation of $CH_3NH_3PbI_3$ layer, CH_3NH_3I (Showa Chemical, 98.8 mg) and PbI_2 (Sigma-Aldrich, 289.3 mg) powders were dissolved in γ-butyrolactone (Wako Pure Chemical Industries, 0.275 mL), and *N*,*N*-dimethylformamide (Sigma-Aldrich, 0.225 mL) was prepared at 60°C. The molar ratio of the solutes is 1 : 1. Three kinds of polysilanes, poly(methyl phenylsilane) (PMPS, Osaka Gas Chemicals, OGSOL SI-10-10, 3 mg), poly(phenylsilane) (PPS, Osaka Gas Chemicals, OGSOL SI-20-10, 3 mg), and decaphenylcyclopentasilane (DPPS, Osaka Gas Chemicals, OGSOL SI-30-10, 3 mg), were used as additives to the perovskite solution, and structures of these polysilanes are shown in Figure 1. In the present work, the perovskite layers are described as $CH_3NH_3PbI_3$, +PMPS, +PPS, and +DPPS. The $CH_3NH_3PbI_3$ solution was spin-coated on the mesoporous TiO_2 layer at 2000 rpm for 60 s. The samples were annealed onto the hot plate at 100°C for 15 min to form a $CH_3NH_3PbI_3$ layer. After cooling to room temperature, hole transport layers were spin-coated. For the hole transport layer, a solution of spiro-OMeTAD (Sigma-Aldrich, 36.1 mg) in chlorobenzene (Wako Pure Chemical Industries, 0.5 mL) was mixed with a solution of lithium bis(trifluoromethylsulfonyl) imide (Li-TFSI, Tokyo Chemical Industry, 260 mg) in acetonitrile (Nacalai Tesque, 0.5 mL) for 12 h. The former solution with 4-tert-butylpyridine (Aldrich, 14.4 μL) was mixed with the Li-TFSI solution (8.8 μL) for 30 min at 70°C. All procedures for preparation of the thin films were carried out in ordinary air. Finally, gold (Au) electrodes were evaporated as top electrodes using a metal mask for the patterning.

The *J-V* characteristics of the photovoltaic devices were measured using a solar simulator composed of light source (San-ei Electric, XES-301S), where solar irradiance of 100 mW cm^{-2} was calibrated before measurements. The measurements were performed by source measure unit (Keysight, B2901A Precision SMU). The scan rate and sampling time were ~0.08 V s^{-1} and 1 ms, respectively. The photovoltaic devices were irradiated through the backside of FTO-coated glass substrate. The effective area of the devices was 0.090 cm^2. IPCE spectra of the devices were also collected using total quantum efficiency solutions for solar cells (Enli Technology, QE-R). The microstructures of the $CH_3NH_3PbI_3$ films were investigated using an X-ray diffractometer (Bruker, D2 PHASER) and an optical microscope (Nikon Eclipse E600). All measurements were performed at room temperature in ambient air.

3. Results and Discussion

Figure 2 shows the *J-V* characteristics of the TiO_2/$CH_3NH_3PbI_3$(polysilane)/spiro-OMeTAD photovoltaic cells under illumination, which indicate the effects of the polysilane addition. Forward and reverse scans are indicated in the figure as indicated by arrows, and the measured photovoltaic parameters (reverse scan) of the present $CH_3NH_3PbI_3$(polysilane) cells are summarized in Table 1. A small hysteresis of reverse and forward scans was observed for the cells. Ordinary

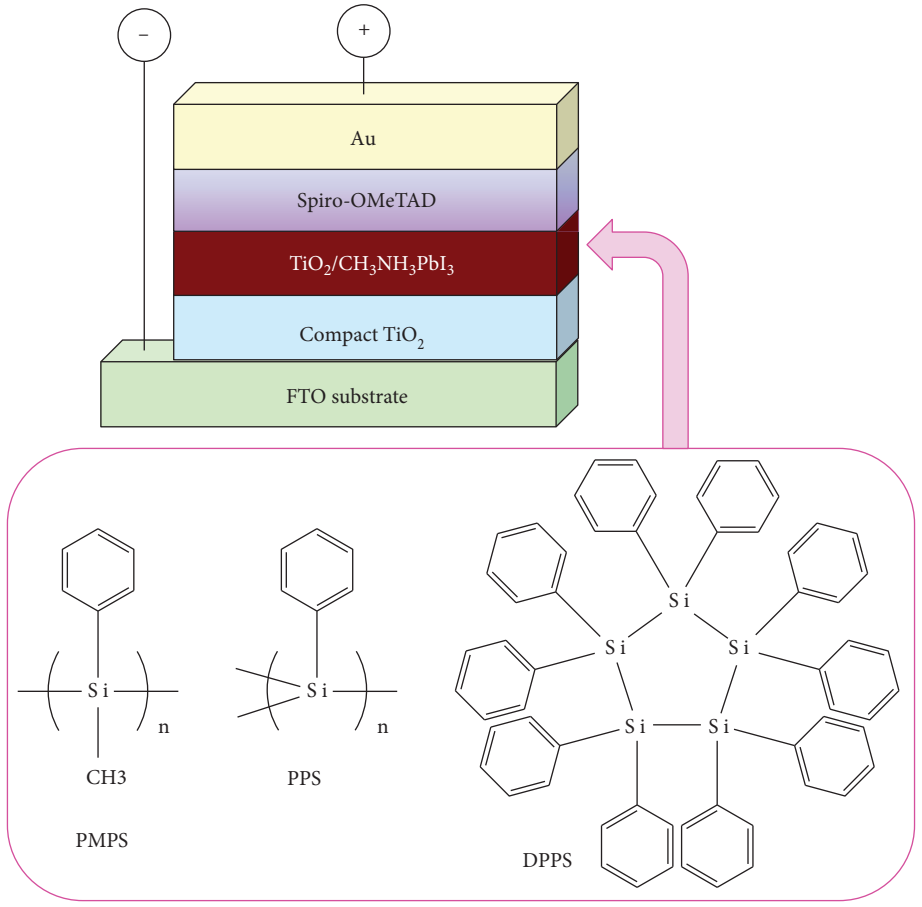

Figure 1: Schematic illustration of the present photovoltaic cells and structure models of the present polysilanes.

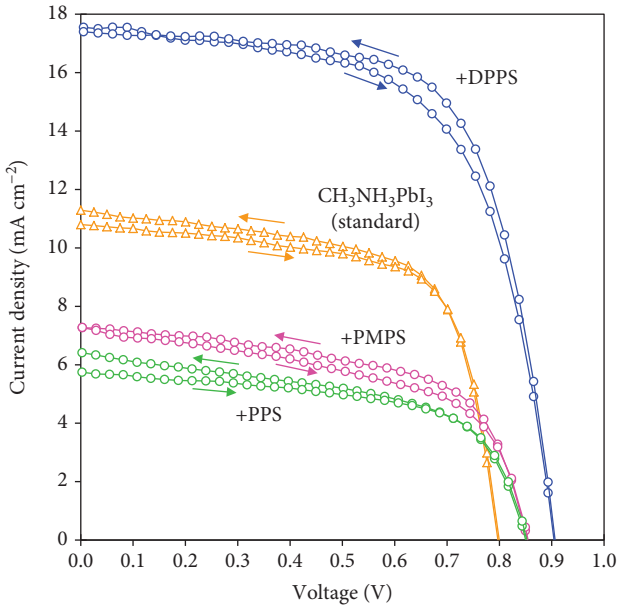

Figure 2: J-V characteristics of $CH_3NH_3PbI_3$ solar cells with polysilanes.

$CH_3NH_3PbI_3$ cells provided a power conversion efficiency (η) of 5.82%, as listed in Table 1. By adding the present three polysilanes, open-circuit voltages (V_{OC}) were increased, as observed in Figure 2. When the PMPS or PPS was added to the perovskite, short-circuit current density (J_{SC}) was decreased. On the other hand, by adding the DPPS, the J_{SC} value and shunt resistance (R_{sh}) were fairly increased, and the series resistance (R_s) was decreased compared with the PMPS and PPS, which resulted in the improvement of the conversion efficiency to 10.46%. The fill factor (FF) is almost the same as that of the ordinary cell.

Figure 3 shows IPCE spectra of the $CH_3NH_3PbI_3$(polysilane) devices. The present cells show photoconversion efficiencies between 320 and 800 nm, which corresponds to an energy gap of 1.55 eV for the $CH_3NH_3PbI_3$ [49]. The IPCE was improved in the range of 400~750 nm by adding DPPS to the perovskite layer, leading to the increase of J_{SC} values, as shown in Figure 2.

Optical microscopic images of ordinary $CH_3NH_3PbI_3$ cell are shown in Figure 4(a), and microparticles with sizes of 5~20 μm are observed. When the polysilanes were added to the perovskite phase, microparticles with homogeneous size distribution were formed, as shown in Figures 4(b)–4(d). In particular, by the DPPS addition, the crystal growth of the perovskite phase was observed, and the distances

Table 1: Measured photovoltaic parameters of $CH_3NH_3PbI_3$ solar cells with polysilanes.

Perovskite layer	J_{sc} (mA cm^{-2})	V_{oc} (V)	FF	R_s (Ω cm^2)	R_{sh} (Ω cm^2)	η (%)
$CH_3NH_3PbI_3$	10.8	0.800	0.674	5.47	700	5.82
+PMPS	7.28	0.855	0.547	9.78	479	3.40
+PPS	5.75	0.852	0.609	11.4	905	2.99
+DPPS	17.4	0.906	0.662	6.13	2190	10.46

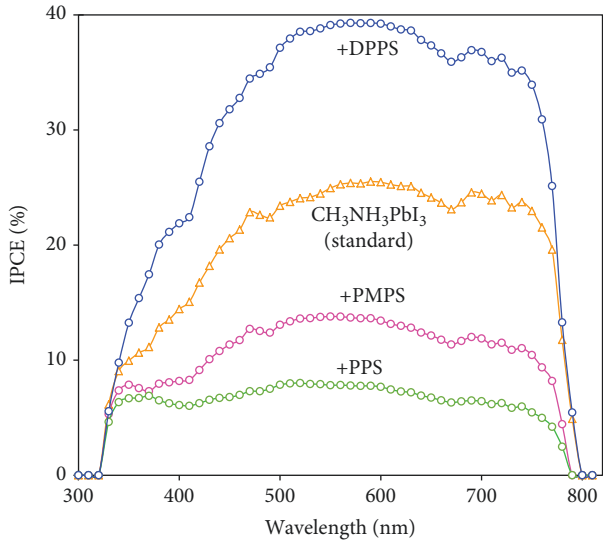

Figure 3: IPCE spectra of $CH_3NH_3PbI_3$ solar cells with polysilanes.

between the particles were decreased, leading formation of more dense microstructures, as observed in Figure 4(d).

Figure 5 shows XRD patterns of the present polysilane-added $CH_3NH_3PbI_3$ solar cells. When the $CH_3NH_3PbI_3$ has a tetragonal structure, an XRD peak corresponding to cubic 200 should be divided into tetragonal 004 and 220, as previously reported in [48]. The calculated XRD pattern also indicates splitting of diffraction reflections of 200 to 004/220 [48], and therefore the diffraction reflections can be indexed by a cubic crystal system ($Pm\bar{3}m$) for the present perovskite thin films. The diffraction peaks indicated by FTO and TiO_2 are from the FTO substrate and TiO_2 mesoporous layer, respectively. For the standard $CH_3NH_3PbI_3$ cell, a diffraction reflection of PbI_2 is observed, as indicated by an arrow. When the polysilanes were added to the perovskite phase, formation of the PbI_2 was suppressed. In addition, peak intensities of 100 of the perovskite phase increased with adding the polysilanes, which indicated crystal growth of the perovskite phase. It is considered that the crystal growth and PbI_2 suppression might be related with affinity between the γ-butyrolactone, *N*,*N*-dimethylformamide, CH_3NH_3I, PbI_2, and polysilanes. X-ray diffraction angles of the perovskite compounds were calibrated based on the 111 reflection of Au [50] of the cell electrodes. The XRD reflections due to the perovskite compounds were measured and indexed to determine the lattice distances. Then, the lattice constants of the perovskite crystals were determined from the lattice distances and indices by using a least squares method (CellCalc program [51]), and they are listed in Table 2. The differences of lattice constants are small and are almost constant for these cells.

Two assumed mechanisms could be considered for the improvement in the photoconversion efficiencies. The first mechanism is the increase and homogenization of the grain sizes of the perovskite crystals by adding polysilanes as observed optical microscopy images in Figure 4. This microstructure promotes the formation of dense interfacial structures and increase of surface coverage. When the grain sizes increase, grain boundary areas that cause carrier scattering decrease, which leads to the increase of the current density [52]. The present homogeneous structure could also suppress the formation of PbI_2, as observed in Figure 5. For the cells with PMPS and PPS, the perovskite domains are isolated, and the cell performances are severely affected by the coverage. Then, the pin holes provide short circuits between n-type semiconductor TiO_2 and p-type semiconductor spiro-MeO-TAD, which resulted in the lower photovoltaic performances.

The second mechanism is the electronic structure change by the polysilanes. By adding polysilanes, the open-circuit voltages increased, as shown in Figure 2. From IPCE spectra in Figure 3, the bandgap energy of the perovskite crystals with PMPS and PPS increased from 1.55 eV to 1.57 eV, which leads to the increase of the V_{OC} values. This also corresponds to the decrease of lattice constants of cubic perovskite by addition of polysilanes. By adding DPPS, on the other hand, the bandgap energy seems to be almost the same as that of the standard perovskite crystal. Since the DPPS has more phenyl groups at the side of Si atoms compared with PMPS and PPS, carrier transport after the carrier separation might be facilitated by π-electrons on the phenyl groups, which affected the increase of IPCE in the range of 400~750 nm and the J_{SC} values. The existence of the phenyl groups might also reduce the electrical resistance of the DPPS-added $CH_3NH_3PbI_3$, which would result in the increase of the V_{OC} values.

Polymer-templated nucleation and growth had been reported as a method for crystal engineering of perovskites [53]. Poly(methyl methacrylate) (PMMA) provided heterogeneous nucleation which would be orders of magnitude faster than the homogeneous nucleation due to the lowering of the nucleation free energy barrier [54]. The PMMA also seems to slow down the growth rate of perovskite crystals by forming an intermediate adduct with PbI_2, which would provide the randomly formed nuclei, and would also lead to smooth thin films with few defects and large oriented perovskite grains [54–56]. The main improvement by the addition of the DPPS is an increase of the film coverage due to enlargement of the perovskite domains as observed in

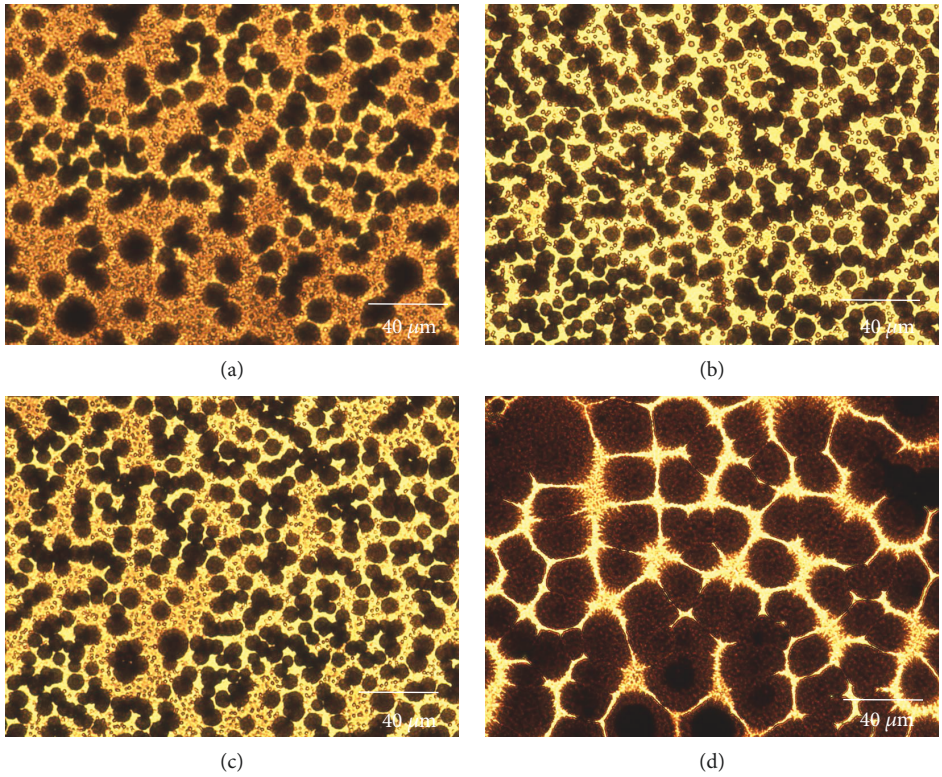

Figure 4: Optical microscopy images of (a) $CH_3NH_3PbI_3$ solar cells with (b) PMPS, (c) PPS, and (d) DPPS.

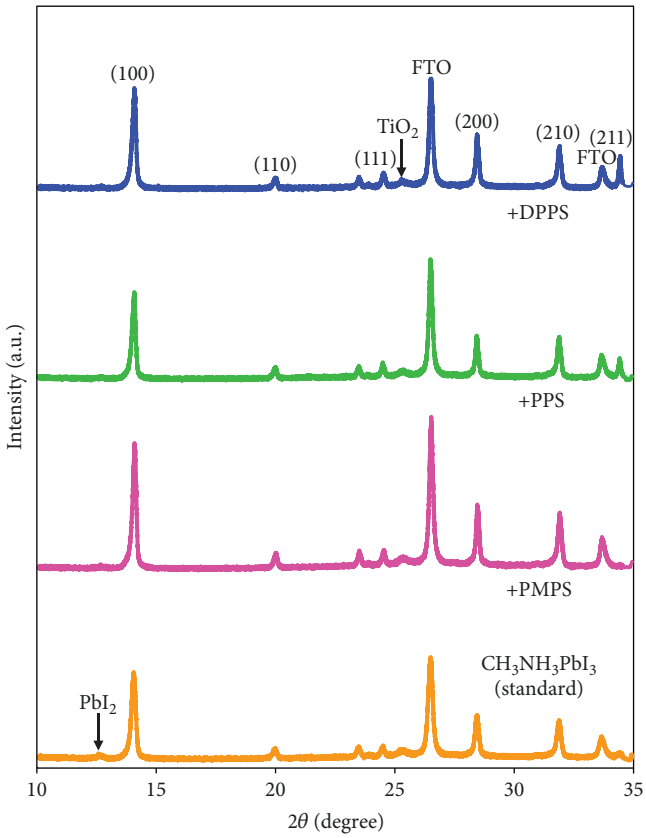

Figure 5: XRD patterns of $CH_3NH_3PbI_3$ solar cells with polysilanes.

Table 2: Measured lattice constants of cubic $CH_3NH_3PbI_3$ perovskite structures with polysilanes.

Perovskite layer	Lattice constant a (Å)
$CH_3NH_3PbI_3$	6.279
+PMPS	6.261
+PPS	6.276
+DPPS	6.276

the optical micrograph of Figure 4(d). Since the DPPS has more phenyl groups at the side of Si atoms compared with PMPS and PPS, molecular interactions created by the phenyl groups would affect the nucleation and crystal growth. Introduction of quantum dots such as PbS [57] or SnS [58] could also control the energy band structure. Further studies are needed for the growth of the perovskite phase and the control of the energy bands.

4. Conclusions

$CH_3NH_3PbI_3$ perovskite solar cells added with polysilanes were fabricated and characterized. Effects of PMPS, PPS, or DPPD addition to perovskite precursor solutions on the photovoltaic properties and the microstructures were investigated. The V_{OC} values were increased by applying these PMPS, PPS, or DPPD, and the IPCE was also increased by the DPPS addition in the range of 400~750 nm, leading to the improvement of the J_{SC} values. Formation of PbI_2 was

also suppressed by the polysilane addition. Microstructure observation of the perovskite layer with DPPS indicated increase of surface coverage to form a dense interfacial structure by grain growth, which resulted in the improvement of conversion efficiencies above 10%. Lots of phenyl group in the DPPS might contribute to the carrier transport in the perovskite layers.

Data Availability

The data used to support the findings of this study are included within the article.

Conflicts of Interest

The authors declare that they have no conflicts of interest.

Acknowledgments

This work was partly supported by the Satellite Cluster Program of the Japan Science and Technology Agency (JST).

References

[1] N. S. Sariciftci, L. Smilowitz, A. J. Heeger, and F. Wudl, "Photoinduced electron transfer from a conducting polymer to buckminsterfullerene," *Science*, vol. 258, no. 5087, pp. 1474–1476, 1992.

[2] M. Granström, K. Petritsch, A. C. Arias, A. Lux, M. R. Andersson, and R. H. Friend, "Laminated fabrication of polymeric photovoltaic diodes," *Nature*, vol. 395, no. 6699, pp. 257–260, 1998.

[3] W. Ma, C. Yang, X. Gong, K. Lee, and A. J. Heeger, "Thermally stable, efficient polymer solar cells with nanoscale control of the interpenetrating network morphology," *Advanced Functional Materials*, vol. 15, no. 10, pp. 1617–1622, 2005.

[4] T. Oku, A. Takeda, A. Nagata et al., "Microstructures and photovoltaic properties of C_{60} based solar cells with copper oxides, $CuInS_2$, phthalocyanines, porphyrin, PVK, nanodiamond, germanium and exciton diffusion blocking layers," *Materials Technology*, vol. 28, no. 1-2, pp. 21–39, 2013.

[5] T. Oku, T. Noma, A. Suzuki, K. Kikuchi, and S. Kikuchi, "Fabrication and characterization of fullerene/porphyrin bulk heterojunction solar cells," *Journal of Physics and Chemistry of Solids*, vol. 71, no. 4, pp. 551–555, 2010.

[6] T. Oku, S. Hori, A. Suzuki, T. Akiyama, and Y. Yamasaki, "Fabrication and characterization of PCBM:P3HT:silicon phthalocyanine bulk heterojunction solar cells with inverted structures," *Japanese Journal of Applied Physics*, vol. 53, no. 5S1, article 05FJ08, 2014.

[7] S. M. Silence, J. C. Scott, F. Hache et al., "Poly(silane)-based high-mobility photorefractive polymers," *Journal of the Optical Society of America B*, vol. 10, no. 12, pp. 2306–2312, 1993.

[8] A. Rybak, J. Jung, W. Ciesielski, and J. Ulanski, "Photovoltaic effect in novel polysilane with phenothiazine rings and its blends with fullerene," *Material Science Poland*, vol. 24, no. 2, pp. 527–534, 2006.

[9] C.-Y. Liu, Z. C. Holman, and U. R. Kortshagen, "Hybrid solar cells from P3HT and silicon nanocrystals," *Nano Letters*, vol. 9, no. 1, pp. 449–452, 2009.

[10] M. Kakimoto, H. Kashihara, T. Kashiwagi, T. Takiguchi, J. Ohshita, and M. Ishikawa, "Visible light photoconduction of poly(disilanyleneoligothienylene)s and doping effect of C_{60}," *Macromolecules*, vol. 30, no. 25, pp. 7816–7820, 1997.

[11] Y. Haga and Y. Harada, "Photovoltaic characteristics of phthalocyanine-polysilane composite films," *Japanese Journal of Applied Physics*, vol. 40, 2A, Part 1, pp. 855–861, 2001.

[12] A. Watanabe and O. Ito, "Photoinduced electron transfer between C_{60} and polysilane studied by laser flash photolysis in the near-IR region," *The Journal of Physical Chemistry*, vol. 98, no. 31, pp. 7736–7740, 1994.

[13] S. Kim, C.-Y. Lee, and M. H.-C. Jin, "Fourier-transform infrared spectroscopic studies of pristine polysilanes as precursor molecules for the solution deposition of amorphous silicon thin-films," *Solar Energy Materials and Solar Cells*, vol. 100, pp. 61–64, 2012.

[14] T. Oku, J. Nakagawa, M. Iwase et al., "Microstructures and photovoltaic properties of polysilane-based solar cells," *Japanese Journal of Applied Physics*, vol. 52, no. 4S, article 04CR07, 2013.

[15] J. Nakagawa, T. Oku, A. Suzuki et al., "Effects of PBr3 addition to polysilane thin films on structures and photovoltaic properties," *Green and Sustainable Chemistry*, vol. 7, no. 1, pp. 20–34, 2017.

[16] A. Kojima, K. Teshima, Y. Shirai, and T. Miyasaka, "Organometal halide perovskites as visible-light sensitizers for photovoltaic cells," *Journal of the American Chemical Society*, vol. 131, no. 17, pp. 6050-6051, 2009.

[17] J.-H. Im, C.-R. Lee, J.-W. Lee, S.-W. Park, and N.-G. Park, "6.5% efficient perovskite quantum-dot-sensitized solar cell," *Nanoscale*, vol. 3, no. 10, pp. 4088–4093, 2011.

[18] H.-S. Kim, C.-R. Lee, J.-H. Im et al., "Lead iodide perovskite sensitized all-solid-state submicron thin film mesoscopic solar cell with efficiency exceeding 9%," *Scientific Reports*, vol. 2, no. 1, 2012.

[19] M. M. Lee, J. Teuscher, T. Miyasaka, T. N. Murakami, and H. J. Snaith, "Efficient hybrid solar cells based on meso-superstructured organometal halide perovskites," *Science*, vol. 338, no. 6107, pp. 643–647, 2012.

[20] J. Burschka, N. Pellet, S.-J. Moon et al., "Sequential deposition as a route to high-performance perovskite-sensitized solar cells," *Nature*, vol. 499, no. 7458, pp. 316–319, 2013.

[21] W. S. Yang, J. H. Noh, N. J. Jeon et al., "Solar cells. High-performance photovoltaic perovskite layers fabricated through intramolecular exchange," *Science*, vol. 348, no. 6240, pp. 1234–1237, 2015.

[22] D. Bi, W. Tress, M. I. Dar et al., "Efficient luminescent solar cells based on tailored mixed-cation perovskites," *Science Advances*, vol. 2, no. 1, article e1501170, 2016.

[23] M. Saliba, T. Matsui, J. Y. Seo et al., "Cesium-containing triple cation perovskite solar cells: improved stability, reproducibility and high efficiency," *Energy and Environmental Science*, vol. 9, no. 6, pp. 1989–1997, 2016.

[24] M. Saliba, T. Matsui, K. Domanski et al., "Incorporation of rubidium cations into perovskite solar cells improves photovoltaic performance," *Science*, vol. 354, no. 6309, pp. 206–209, 2016.

[25] Z. Tang, T. Bessho, F. Awai et al., "Hysteresis-free perovskite solar cells made of potassium-doped organometal halide perovskite," *Scientific Reports*, vol. 7, no. 1, p. 12183, 2017.

[26] S. D. Stranks, G. E. Eperon, G. Grancini et al., "Electron-hole diffusion lengths exceeding 1 micrometer in an organometal trihalide perovskite absorber," *Science*, vol. 342, no. 6156, pp. 341–344, 2013.

[27] D. Shi, V. Adinolfi, R. Comin et al., "Low trap-state density and long carrier diffusion in organolead trihalide perovskite single crystals," *Science*, vol. 347, no. 6221, pp. 519–522, 2015.

[28] Q. Dong, Y. Fang, Y. Shao et al., "Electron-hole diffusion lengths > 175 μm in solution-grown $CH_3NH_3PbI_3$single crystals," *Science*, vol. 347, no. 6225, pp. 967–970, 2015.

[29] T. Oku, Y. Ohishi, A. Suzuki, and Y. Miyazawa, "Effects of NH_4Cl addition to perovskite $CH_3NH_3PbI_3$ photovoltaic devices," *Journal of the Ceramic Society of Japan*, vol. 125, no. 4, pp. 303–307, 2017.

[30] T. Oku and Y. Ohishi, "Effects of annealing on $CH_3NH_3PbI_3$(cl) perovskite photovoltaic devices," *Journal of the Ceramic Society of Japan*, vol. 126, no. 1, pp. 56–60, 2018.

[31] F. Hao, C. C. Stoumpos, D. H. Cao, R. P. H. Chang, and M. G. Kanatzidis, "Lead-free solid-state organic–inorganic halide perovskite solar cells," *Nature Photonics*, vol. 8, no. 6, pp. 489–494, 2014.

[32] W. Liao, D. Zhao, Y. Yu et al., "Fabrication of efficient low-bandgap perovskite solar cells by combining formamidinium tin iodide with methylammonium lead iodide," *Journal of the American Chemical Society*, vol. 138, no. 38, pp. 12360–12363, 2016.

[33] T. Krishnamoorthy, H. Ding, C. Yan et al., "Lead-free germanium iodide perovskite materials for photovoltaic applications," *Journal of Materials Chemistry A*, vol. 3, no. 47, pp. 23829–23832, 2015.

[34] Y. Ohishi, T. Oku, and A. Suzuki, "Fabrication and characterization of perovskite-based $CH_3NH_3Pb_{1-x}Ge_xI_3$, $CH_3NH_3Pb_{1-x}Tl_xI_3$ and $CH_3NH_3Pb_{1-x}In_xI_3$ photovoltaic devices," *AIP Conference Proceedings*, vol. 1709, no. 1, article 020020, 2016.

[35] T. Oku, Y. Ohishi, and A. Suzuki, "Effects of antimony addition to perovskite-type $CH_3NH_3PbI_3$ photovoltaic devices," *Chemistry Letters*, vol. 45, no. 2, pp. 134–136, 2016.

[36] T. Oku, Y. Ohishi, A. Suzuki, and Y. Miyazawa, "Effects of Cl addition to Sb-doped perovskite-type $CH_3NH_3PbI_3$ photovoltaic devices," *Metals*, vol. 6, no. 7, p. 147, 2016.

[37] J. Zhang, M.-H. Shang, P. Wang et al., "n-type doping and energy states tuning in $CH_3NH_3Pb_{1-x}Sb_{2x/3}I_3$ perovskite solar cells," *ACS Energy Letters*, vol. 1, no. 3, pp. 535–541, 2016.

[38] T. Oku, Y. Ohishi, and A. Suzuki, "Effects of $SbBr_3$ addition to $CH_3NH_3PbI_3$ solar cells," *AIP Conference Proceedings*, vol. 1807, no. 1, article 020007, 2017.

[39] Y. Ando, T. Oku, and Y. Ohishi, "Rietveld refinement of crystal structure of perovskite $CH_3NH_3Pb(Sb)I_3$ solar cells," *Japanese Journal of Applied Physics*, vol. 57, no. 2S2, article 02CE02, 2018.

[40] T. Oku, M. Zushi, K. Suzuki, Y. Ohishi, T. Matsumoto, and A. Suzuki, "Nanostructured solar cells," in *Fabrication and characterization of element-doped perovskite solar cells*, N. Das, Ed., pp. 217–243, InTech, Croatia, 2017.

[41] Y. Shirahata and T. Oku, "Effects of copper addition on photovoltaic properties of perovskite $CH_3NH_3PbI_{3-x}Cl_x$ solar cells," *Physica Status Solidi A*, vol. 214, no. 10, 2017.

[42] Y. Shirahata and T. Oku, "Microstructures, optical and photovoltaic properties of $CH_3NH_3PbI_{3(1-x)}Cl_x$ perovskite films with CuSCN additive," *Materials Research Express*, vol. 5, no. 5, 2018.

[43] T. Oku, Y. Ohishi, and H. Tanaka, "Effects of CuBr addition to $CH_3NH_3PbI_3$(Cl) perovskite photovoltaic devices," *AIP Conference Proceedings*, vol. 1929, no. 1, article 020010, 2018.

[44] H. Tanaka, Y. Ohishi, and T. Oku, "Effects of Cu addition to perovskite $CH_3NH_3PbI_{3-x}Cl_x$ photovoltaic devices with hot airflow during spin-coating," *Japanese Journal of Applied Physics*, vol. 57, no. 8S3, article 08RE10, 2018.

[45] T. Hamatani and T. Oku, "Effects of halide addition to arsenic-doped perovskite photovoltaic devices," *AIP Conference Proceedings*, vol. 1929, no. 1, article 020018, 2018.

[46] H. Tanaka, T. Oku, and N. Ueoka, "Structural stabilities of organic–inorganic perovskite crystals," *Japanese Journal of Applied Physics*, vol. 57, no. 8S3, article 08RE12, 2018.

[47] Y. Shirahata, Y. Yamomoto, A. Suzuki, T. Oku, S. Fukunishi, and K. Kohno, "Effects of polysilane-doped spiro-OMeTAD hole transport layers on photovoltaic properties," *Physica Status Solidi A*, vol. 214, no. 3, 2017.

[48] T. Oku, M. Zushi, Y. Imanishi, A. Suzuki, and K. Suzuki, "Microstructures and photovoltaic properties of perovskite-type $CH_3NH_3PbI_3$ compounds," *Applied Physics Express*, vol. 7, no. 12, p. 121601, 2014.

[49] T. Oku, *Solar Cells and Energy Materials*, Walter de Gruyter, Berlin, 2017.

[50] M. Ellner, K. Kolatschek, and B. Predel, "On the partial atomic volume and the partial molar enthalpy of aluminium in some phases with Cu and Cu_3Au structures," *Journal of the Less Common Metals*, vol. 170, no. 1, pp. 171–184, 1991.

[51] H. Miura, "CellCalc: a unit cell parameter refinement program on Windows computer," *Nihon Kessho Gakkaishi*, vol. 45, no. 2, pp. 145–147, 2003.

[52] W. Nie, H. Tsai, R. Asadpour et al., "Solar cells. High-efficiency solution-processed perovskite solar cells with millimeter-scale grains," *Science*, vol. 347, no. 6221, pp. 522–525, 2015.

[53] D. Bi, C. Yi, J. Luo et al., "Polymer-templated nucleation and crystal growth of perovskite films for solar cells with efficiency greater than 21%," *Nature Energy*, vol. 1, no. 10, 2016.

[54] A. Cacciuto, S. Auer, and D. Frenkel, "Onset of heterogeneous crystal nucleation in colloidal suspensions," *Nature*, vol. 428, no. 6981, pp. 404–406, 2004.

[55] T. Oku, Y. Ohishi, and N. Ueoka, "Highly (100)-oriented $CH_3NH_3PbI_3$(Cl) perovskite solar cells prepared with NH_4Cl using an air blow method," *RSC Advances*, vol. 8, no. 19, pp. 10389–10395, 2018.

[56] N. Ueoka, T. Oku, H. Tanaka et al., "Effects of PbI_2 addition and TiO_2 electron transport layers for perovskite solar cells," *Japanese Journal of Applied Physics*, vol. 57, no. 8S3, p. 08RE05, 2018.

[57] Y. Yang and W. Wang, "Effects of incorporating PbS quantum dots in perovskite solar cells based on $CH_3NH_3PbI_3$," *Journal of Power Sources*, vol. 293, pp. 577–584, 2015.

[58] J. Han, X. Yin, H. Nan et al., "Enhancing the performance of perovskite solar cells by hybridizing SnS quantum dots with $CH_3NH_3PbI_3$," *Small*, vol. 13, no. 32, article 1700953, 2017.